Desalination and Water Treatment
www.deswater.com
doi: 10.5004/dwt.2022.28141

252 (2022) 219–232
March

Magnetic carbon nanocomposite derived from waste tire rubber for atrazine removal from aqueous solutions

N. Heydarian Dana[a], M. Borghei[b,*], A. Takdastan[c], A.H. Javid[d], M.A. Zazouli[e]

[a]*Department of Environmental Engineering, Tehran Science and Research Branch, Islamic Azad University, Tehran, Iran, email: Heydarian.Nahid@gmail.com*
[b]*Department of Chemical and Petroleum Engineering, Sharif University of Technology, Tehran, Iran, email: mborghei2@sharif.edu*
[c]*Department of Environmental Technologies Research Center, Ahvaz Jundishapur University of Medical Sciences, Ahvaz, Iran, email: Afshin_ir@yahoo.com*
[d]*Department of Environmental Engineering, Graduate School of the Environment and Energy, Islamic Azad University, Science and Research Campus, Tehran, Iran, email: ahjavid@gmail.com*
[e]*Department of Environmental Health, Health Sciences Research Center, Faculty of Health, Mazandaran University of Medical Sciences, Sari, Iran, email: zazoli49@yahoo.com*

Received 26 May 2021; Accepted 19 December 2021

ABSTRACT

In this study magnetite nanoparticles (Fe_3O_4) were synthesized and embedded in activated carbon (AC) derived from waste tire rubber to produce magnetic activated carbon. The atrazine ($C_8H_{14}ClN_5$) adsorption was performed over (AC/Fe_3O_4) nanocomposite in an aqueous solution and adsorption isotherms and kinetics were determined. The effects of some parameters such as (pH, contact time, adsorbent dosage and initial pesticide concentration) were investigated. Characterization of nanocomposite was carried out by high-resolution scanning electron microscopy and transmission electron microscopy, X-ray powder diffraction, vibrating sample magnetometer, Brunauer–Emmett–Teller, Fourier-transform infrared spectroscopy (FTIR), energy-dispersive X-ray spectroscopy, and zeta potential analyses. The characterization results showed that the synthesized composite has a mesoporous cubic structure along with narrow size distribution of uniform Fe_3O_4 particles in the carbon matrix. The composite showed super magnetic behavior considering to its low coercivity (2.44 Qe) and high saturation magnetization (36.43 emu g^{-1}). The FTIR spectra exhibited successful bonding of iron ions on activated carbon surface. The adsorption study showed that the atrazine concentration reached to equilibrium after 220 min, and the optimum atrazine removal was 76% at pH = 8, 1 g L^{-1} adsorbent dosage, and 15 mg L^{-1} of atrazine concentration. The adsorption data fitted Langmuir model and showed a higher correlation with pseudo-second-order reaction.

Keywords: Atrazine; Adsorption process; Magnetic nanocomposite; Aqueous solutions; Waste tire rubber; Persistent organic pollutant

1. Introduction

Pesticides are classified as persistent organic pollutants (POPs) and thus their removal has received an increasing attention recently. Atrazine (2-chloro, 4 ethylamino, 6 isopropyl amino, S-triazine) is a non-selective pesticide which is the most detected one in runoff and surface waters [1,2]. Atrazine (ATZ) is highly resistant in soil and has a long half-life ranged from 13 to 261 d and causes a dramatic decline in soil flora and fauna. Low vapor pressure and moderate water solubility (33 mg L^{-1} at 20°C) made ATZ an unpreventable ground water contamination. ATZ reduces the

* Corresponding author.

dissolved oxygen and pH of the water bodies, increases the calcium and is the leading cause of death in macrophytes and other aquatic species [3,4]. Due to its heterocyclic structure participates in S_NAr[1] reaction and hence ATZ has been considered as a carcinogenic material by USEPA, and EU banned its usage from 2004. Potable water is the main source of human exposure to the ATZ and short-term use of water containing it more than maximum contaminant level (MCL) can lead to chronic obstructive pulmonary disease (COPD), kidney failure, muscle spasm, weight loss, and changing the conformation of human serum albumin (HAS). Additionally, ATZ is an endocrine disruptor and long-term exposure causes adrenal harm and macular degeneration (MD) [5–8].

Several methods have been suggested for ATZ removal comprises biological treatment [9–11], anaerobic digestion [12], phytoremediation [13]; and physicochemical procedures such as reverse osmosis [14], electrooxidation [15] incineration, nanomembrane filtration [16], and ultra-sonic destruction [17]. All mentioned methods suffer drawbacks like having low yield, high cost of energy, prolonged reaction time, and toxic metabolites and they are also not eco-friendly. Lately there has been a trend towards exploiting nanomaterials for applications like wastewater purification due to their unique properties and therefore a lot of studies have been carried out for carbon-based nano-adsorbents fabrication. Adsorption with activated carbon (AC) and carbon nanotubes (CNT) and other carbonous composites is an effective technique for removing pollutants in water bodies such as metals like arsenic [18], chromium [19] and mercury [20] and non-metal pollutions like fluoride [21] methylene blue [22] methyl orange [23] rhodamine B [24] and organic pollutants like nonylphenol and atrazine [25–27]. AC with it is large surface area is capable of adsorbing suspended solids, soluble gas in liquids, heavy metals from aqueous media, phenols, dyes, aromatics, butane, and nitrogen oxides (NO_X) gases. AC is derived from materials containing high amounts of carbon like char, lignin, wood and organic polymers. Over recent years, researchers showed heightened interest in recycling wastes like sawdust, paper milling sludge, and particularly waste tire which consist largely of black carbon to produce the AC. Waste tires are composed of 62 wt.% styrene butadiene rubber tire (SBR), 31% black carbon and are more favorable to synthesize AC through pyrolysis [28,29].

However, using nanoscale colloidal adsorbents requires a delicate separation process after decontamination. The magnetic particles have developed to tackle this problem since they are readily separable and do not need filtration, solid phase extraction columns or additional operations. Considering their low toxicity to humans and nature, Fe_3O_4 nanoparticles are the most common used magnetic particles among the others [30]. They possess beneficial features like super magnetism and functional modification [31]. Nevertheless, magnetite nanoparticles are easily oxidized in air and aggregate in solution, hence they should be modified with organic polymers, carbon nanomaterials and metals [32]. In this work, we firstly synthesized activated carbon from waste tire granules and fabricated a magnetic composite by coating Fe_3O_4 nanoparticles with AC via co-precipitation method. The products were characterized by Fourier-transform infrared spectroscopy (FTIR), X-ray powder diffraction (XRD), scanning electron microscopy (SEM), transmission electron microscopy (TEM), vibrating sample magnetometer (VSM), Brunauer–Emmett–Teller (BET), and energy-dispersive X-ray spectroscopy (EDS) and the powder used for atrazine adsorption in aqueous solution.

2. Material and methods

2.1. Chemicals and reagents

All the chemicals used in the present investigation were of analytical reagent grade (purity > 99%) and used without any further purification. Atrazine ($C_8H_{14}ClN_5$), methanol (CH_3OH), hydrochloric acid (HCl), sodium hydroxide (NaOH), ferric chloride ($FeCl_3{\cdot}6H_2O$), ferro chloride ($FeCl_2{\cdot}4H_2O$), and ammonium hydroxide ($NH_3{\cdot}H_2O$ 25%) were purchased from Merck and Sigma-Aldrich Companies. Deionized water was prepared from Merck Millipore instrument. Passenger car tire granules was purchased from a local industry for pyrolysis and according to the brochure, ground granules contained 69.7 wt.% of volatile content, 21.3 wt.% of fixed carbon, 8.3 wt.% ash and 0.7 wt.% moisture.

2.2. Preparation of activated carbon

The activated carbon was prepared based on the study of Gupta et al. [33]. Tire granules washed with distilled water and dried for 2 h at 100°C. The carbonization was done by heating at 500°C for 5 h and followed by immersing in hydrogen peroxide at 60°C for 24 h to oxidize the organic impurities. The material was washed 3 times with deionized water and vacuum dried at 110°C for 2 h. The activation of the powder was done by heating at 900°C for 2 h at a muffle furnace and the product was soaked of the ashes by washing with HCl 1 M and eventually dried at 100°C for 2 h.

2.3. Synthesis of magnetic carbon nanocomposite (AC/Fe_3O_4)

Synthesizing of AC/Fe_3O_4 nanoparticles was done via co-precipitation process. This work was accomplished by dissolving $FeCl_3{\cdot}6H_2O$ and $FeCl_2{\cdot}4H_2O$ precursors with (4:1) molar ratio in 400 mL of degassed deionized water under nitrogen gas at 80°C and the mixture stirred for 45 min. 10 g of prepared activated carbon and 50 mL of $NH_3{\cdot}H_2O$ (25%) were subsequently added to the solution. Afterwards, it was heated and mixed with 400 rpm for 30 min. Finally produced composite was separated with magnet and washed with distilled water consecutively. For drawing an analogy between the magnetic properties of composite and magnetite, the magnetite nanoparticles were separately synthesized according to the literature [34]. The as prepared Fe_3O_4 powder was stored in vacuum storage container before use.

2.4. Characterization of nanocomposite

X-ray diffraction instrument (XRD Philips pw3710, kα co = 1.79 Å) was employed to confirm the presence of

[1] Nucleophilic aromatic substitution

favorable phases. The powder samples were pressed into the sample holder and scanned from 20° to 80° at a scan rate of 8°min^{-1} and 40 kV of bias voltage. The surface functional groups of AC, AC/Fe_3O_4 before and after ATZ adsorption were determined by employing thermo AVATAR FTIR instrument. The samples were prepared by mixing with potassium bromide (KBr) powder at the ratio of 1:10 and pressed under the pressure of 11 tons in the holder for 3 min and the pellets were placed in the sample compartment for analysis. Spectra were recorded from 4,000 to 400 cm^{-1} at a resolution of 2 cm^{-1} at room temperature and a pressure of <1 mbar. The surface morphology and microstructure of synthesized AC and composite were studied through scanning electron microscopy & high-resolution scanning electron microscopy (SEM & HRSEM, TESCAN miraIII) using a secondary electron detector. The powder sample was mounted on a carbon tape on an aluminum stub and followed by gold coating, moreover the transmission electron microscopy (TEM, Zeiss Em900) applied to analyze the morphology and particles distribution precisely. The energy-dispersive X-ray analysis was employed for determination of surface elemental composition with the SEM device. The BET surface area of the powder measured by N_2 adsorption/desorption isotherms with Belsorp mini II instrument. Two processes of degassing for purifying adsorbent from water and volatile compounds was done by heating at 100°C (1 h) and 400°C (3 h). The evaluation of magnetic properties of Fe_3O_4 nanoparticles and magnetic composite was done by VSM technique on Microsense ev9. The surface potential charge of composite was measured by using zeta potential instrument (Horiba SZ-100) at various pH values. For studying the pH_{zpc}, 50 mL of NaCl (0.01 M) used as electrolyte solution and was poured in 10 Erlenmeyer flasks and the pH adjusted with HCl 0.1 N and NaOH 0.1 N and a constant amount of adsorbent was added to each flask. After 48 h of contact time on a shaker with 150 rpm, the pH values were red.

2.5. Adsorption experiments

At first, a stock solution with concentration of 1,000 mg L^{-1} of atrazine prepared by dissolving 1 g ATZ in 1,000 mL of ethanol and diluted in deionized water for the subsequent experiments. All atrazine adsorption experiments were conducted batch adsorption method in 100, 250 mL Erlenmeyer on a shaking water bath (Sheldon SWBR27) with 150 rpm at 20°C. The amount of adsorbed atrazine (mg) per composite mass (g) is calculated as follows:

$$Q = \frac{x}{m} = \frac{\left(C_0 - C_t\right) V}{m} \tag{1}$$

where C_0 and C_t are the initial and final concentration of atrazine in the solution (mg L^{-1}) respectively, V is the volume solution (L) and W(g) is the weight of adsorbent. For investigating the kinetic, adsorption isotherms, contact time and equilibrium concentration, the atrazine solutions with concentrations of 2, 5, 10, 15, 20 and 25 mg L^{-1} were prepared and experiments were conducted at different pH at 400 min of reaction time. A 5 mL of sample from each flask was taken at 10 min intervals and a centrifuge with 4,000 rpm used to spin out the adsorbent after separating with magnet and the remnant atrazine concentration at the supernatant was measured.

Langmuir and Freundlich isotherms were used for adsorption at one temperature (20°C). Langmuir isotherm was modelled on the assumption that the adsorption occurs on homogenous site and Freundlich isotherm employed when the adsorption takes place on heterogeneous sites of the adsorbent and thus the type of the adsorption can be determined by studying these isotherms. The Langmuir and Freundlich equations are presented as follow:

$$\frac{1}{q_e} = \frac{1}{kq_0} \times \frac{1}{c_e} + \frac{1}{q_0} \tag{2}$$

$$\log Q_e = \log K_f + \frac{1}{n} \log C_e \tag{3}$$

where q_e and q_0 (mg g^{-1}) are adsorbed atrazine at equilibrium and at initial time (min), and k, K_f are the rate constant of the Langmuir and Freundlich equations. The atrazine adsorption kinetic was evaluated by pseudo-first-order and second-order reactions presented in Eqs. (4) and (5).

$$\log Q_e = \log K_f + \frac{1}{n} \log C_e \tag{4}$$

$$\frac{t}{q_t} = \frac{1}{k_2 q_e^2} + \frac{1}{q_e t} \tag{5}$$

where q_e and q_t (mg g^{-1}) are adsorbed atrazine at equilibrium and at time (min) and k_1 and k_2 are the first and second-order constant rates. To investigate the regeneration capability, the adsorbent was washed repeatedly with methanol (99%) and deionized water by the end of each cycle and vacuum dried followed by drying in an oven at 80°C for 4 h.

2.6. Analytical procedures

The ATZ concentrations were monitored by high performance liquid chromatography (HPLC, KNAUER Wellchrom) equipped with UV detector at 222 nm. A C18 column (Hector-M) was utilized as a back phase for separation and the mobile phase was a mixture of water and methanol (80:20) with a flow rate of 0.5 mL min^{-1}. The iron contents of the samples were detected by inductively coupled plasma-optical emission spectrometry (ICP-OES).

3. Results and discussion

3.1. Characterization of synthesized nanocomposites

3.1.1. XRD patterns

Fig. 1 shows the X-ray diffraction patterns of the adsorbent and as synthesized nanoparticles which is in compliance with magnetite reference JCPDS (96-900-0927) and cubic structure with (d_{111} = 0.48 nm, d_{220} = 0.297 nm, d_{311} = 0.25 nm, d_{222} = 0.24 nm) [33,35]. The impurities peaks in 2θ = 31°, 37° of the adsorbent pattern could be related to the graphite. Crystalline size was calculated 44.8 nm with full width

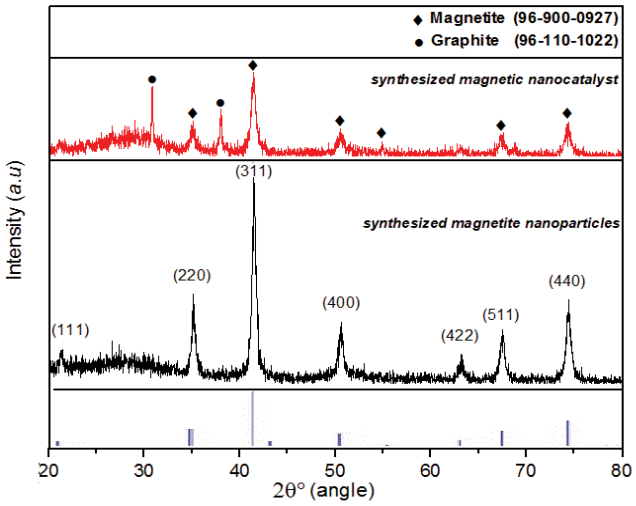

Fig. 1. XRD pattern of magnetite and magnetic adsorbent.

at half maximum (FWHM) using Debye–Scherer equation presented below:

$$T = \frac{K\lambda}{\beta\cos\theta} \tag{6}$$

where T is mean size of the ordered crystalline, K is a dimensionless factor (with value of 0.9), λ is X-ray wavelength, β is the line broadening at half maximum (FWHM) and θ is the Bragg angle.

3.1.2. Fourier-transform infrared spectroscopy

The FTIR spectra of AC and AC/Fe_3O_4 before and after adsorption are depicted in Fig. 2. The peaks at 1,103 and 1,568 cm^{-1} are assigned to the C–O and O–H stretching vibration respectively [36,37]. All 3 samples showed characteristic peaks of C=C stretching and O–H stretching around 1,600 and 3,400 cm^{-1}. The peaks at 1,567 cm^{-1} is attributed to the stretching of C=C bond which is characteristic of graphite and also could be assigned to the deformation vibrating of adsorbed water molecules to the KBr tablets [36–39]. The broad peak ranging from 2,900 to 3,700 cm^{-1} might be the overlapping peaks related to the O–H and C–C stretching vibrational mode and also asymmetric vibration of C–H bonds [37,40]. The finger print area (500–1,800 cm^{-1}) have several peaks and the sharp peaks in both composites at 579.8 cm^{-1} correspond to the Fe–O stretching vibration which conform the successful loading of Fe_3O_4 on the surface of AC and iron ion stability after ATZ adsorption [37,39,41–43]. The peak at 1,729 cm^{-1} arose from axial deformation vibrations CO of aryl halide indicating the adsorption of triazine ring by adsorbent. Moreover, the stretching vibration of C–C–O at 1,270 cm^{-1} shows the presence of alcohols after adsorption and it has to be noted that the solvent of atrazine is methanol [44].

3.1.3. Electron microscopy

Fig. 3a indicates the HRSEM graph of the composite in secondary electron mode and shows agglomerated particles with spherical morphology and Fig. 3b exhibits the uniform distribution of Fe_3O_4 particles in composite. The brighter spots in Fig. 3b represent iron oxides. Moreover, the particle size did not exceed 100 nm and it has a good distribution (Fig. 5b) and proper porosity for adsorption of pollutants. The backscatter electron mode graph of Fig. 3c confirms the spherical morphology for AC/Fe_3O_4. By calculation in the same figure, the average particles size is 52 nm which is relatively consistent with the XRD data [34]. The EDS graph in Fig. 5a confirms the presence of 30 wt.% of iron element on the carbon surface. The SEM micrograph of magnetite nanoparticles which are synthesized separately is presented in Fig. 4a and b and indicates semi-cubic shape for magnetite. In comparison with in-situ synthesized, these nanoparticles had larger size owing to the temperature condition of synthesis process and also the lack of growth and oxidizing inhibitor. Hence, co-precipitation with carbon lead to decrease the particle size. Furthermore, TEM analysis in Fig. 6 shows uniform spherical particles of composite with size span from 40 to 70 nm. In this figure the gray areas belong to the AC and dimmer spots indicates the Fe_3O_4 particles.

3.1.4. BET surface areas and pore distributions

The adsorption/desorption isotherms of the activated carbon and magnetic adsorbent in 77°K are shown in Fig. 7 and on the basis of the IUPAC classification, the isotherm is of II type which shows multilayer adsorption on a powerful macro pore adsorbent [45]. Similar results are obtained in other work [46]. The BET results presented in Table 1 shows a decline in surface area from 193 to 111 $m^2\ g^{-1}$ due to the occupying the pores on the surface of the adsorbent and substitution with iron oxide [47].

3.1.5. Magnetic properties

The adsorbent magnetic property was measured in an applied field from –5 KQe to 5 KQe and Fig. 8 shows hysteresis loop for adsorbent and magnetite. The saturation magnetization (Ms) achieved 36.43 and 55. 68 emu g^{-1} for adsorbent and iron oxide nanoparticles respectively. Given that the Ms for magnetite has amounts ranging from 70 to 90 emu g^{-1}, thus the as synthesized magnetite nanoparticles might well have impurities like maghemite (γFe_2O_3) [48], however, decreasing the size of nanoparticles can lead to decline in saturation value of the magnetization [49]. Considering the value of Ms and low amount of coercivity presented in Table 2, the adsorbent has super-paramagnetic property [50].

3.1.6. pH_{zpc} and zeta potential

Atrazine is naturally neutral and has weak interplay with surface of the AC like Van Der Waals, hydrogen bond and hydrophobic interactions [51]. Nonetheless, analyzing the zero-point charge helps to comprehend the atrazine reaction with adsorbent surface. The isoelectric point is of importance since the surface charge is zero and at higher pH values the surface will be charged negatively and absorb positive particles, and vice versa. According to the diagram

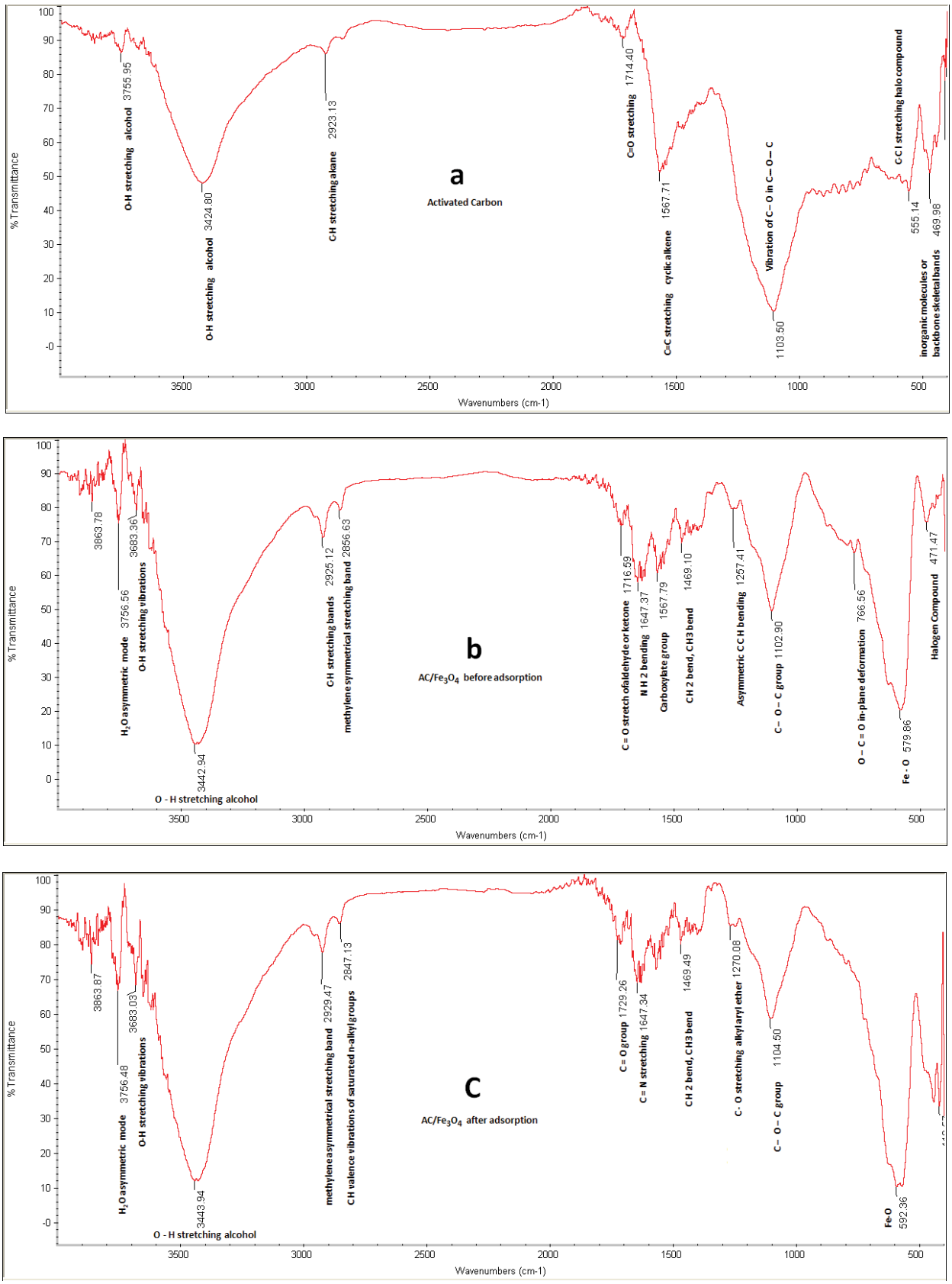

Fig. 2. FTIR spectra of (a) activated carbon (b and c) composite before and after adsorption.

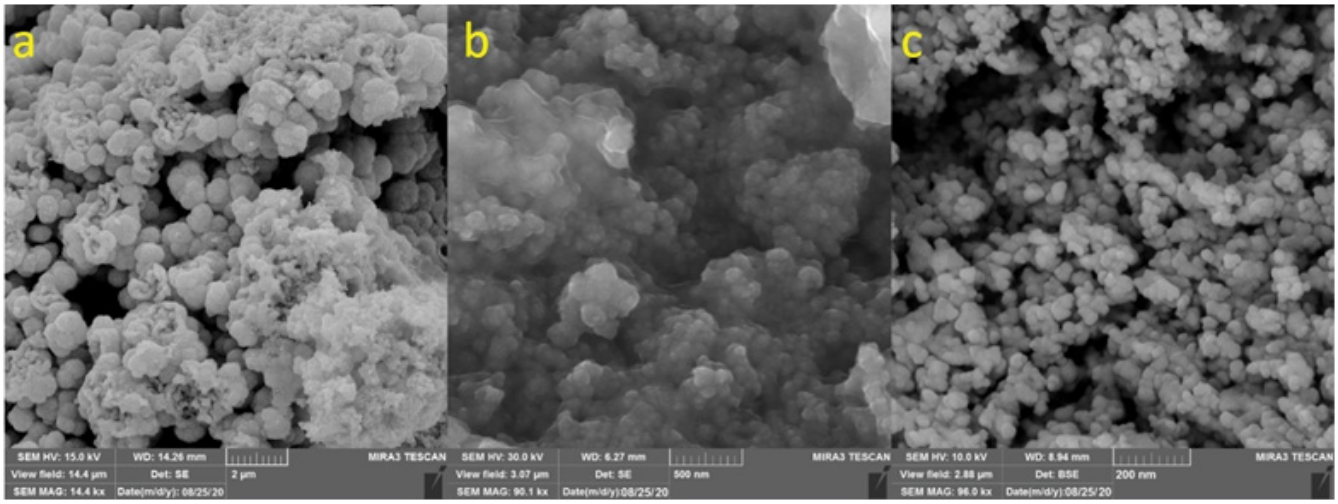

Fig. 3. (a and b) secondary electron mode HRSEM and (c) back scatter mode HRSEM of adsorbent.

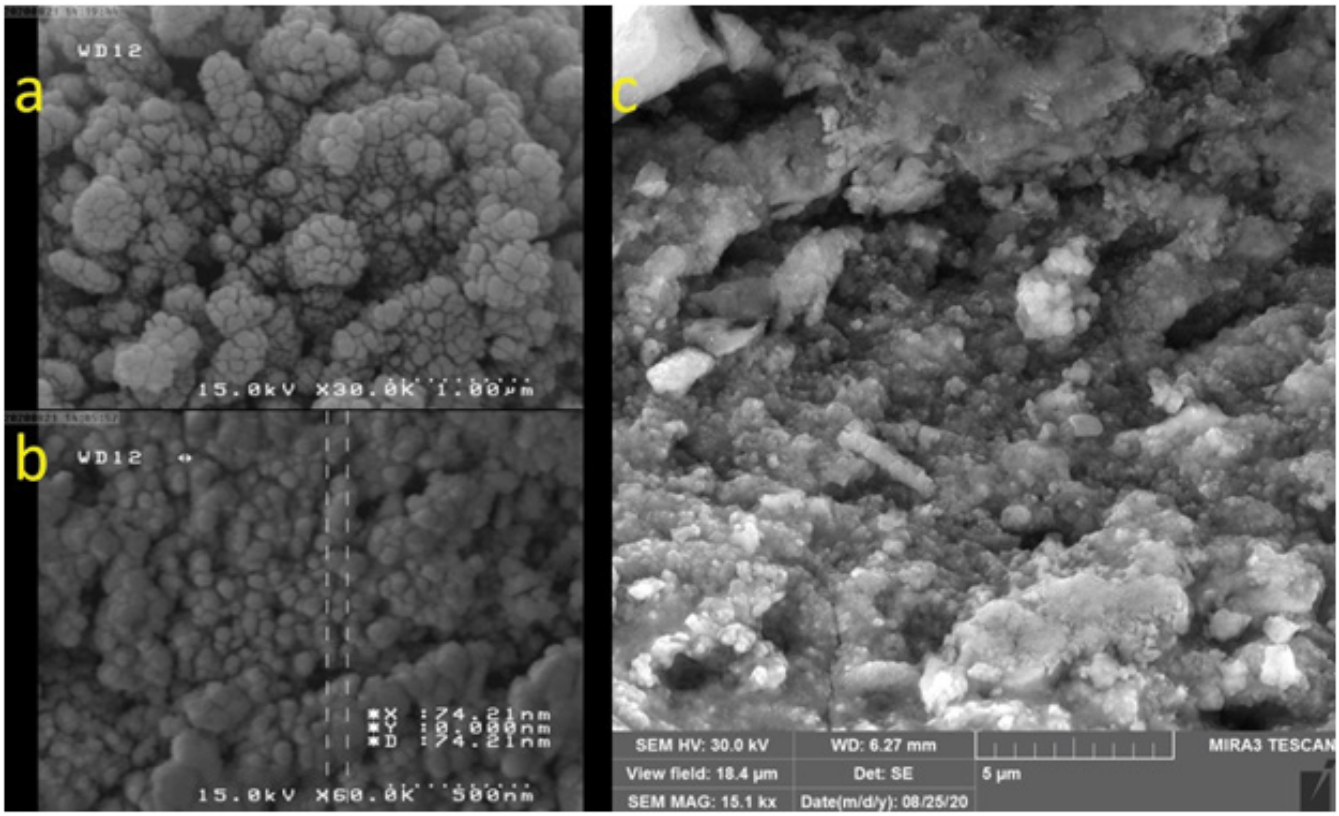

Fig. 4. (a and b) SEM of Fe_3O_4 nanoparticles without modification and (c) reused composite.

in Fig. 9a, the zpc pH ranges in value from 6 to 8 and the best point with identical initial and final pH was achieved 7.93. The zeta potential of the composite was measured at pH ranging from 3 to 10. Fig. 9b depicts the fluctuations of zeta potential from 3·3 mV at pH = 3 to –25 mV at pH = 10 which indicates the stability of particles in aqueous media. The zero-point charge was observed at pH = 6.8 and the differences between two measured numbers could be due to the different experiment conditions.

3.2. Process optimization

3.2.1. Effect of pH

The effect of pH values from 2–12, was studied through conducting batch adsorption experiments by 20 mg L^{-1} of ATZ and 1 g L^{-1} of adsorbent at 100 min of reaction time. The graph of Fig. 10a and b show ascending order for adsorption capacity and removal efficiency while the pH approaches to 8 and descending afterwards and therefore

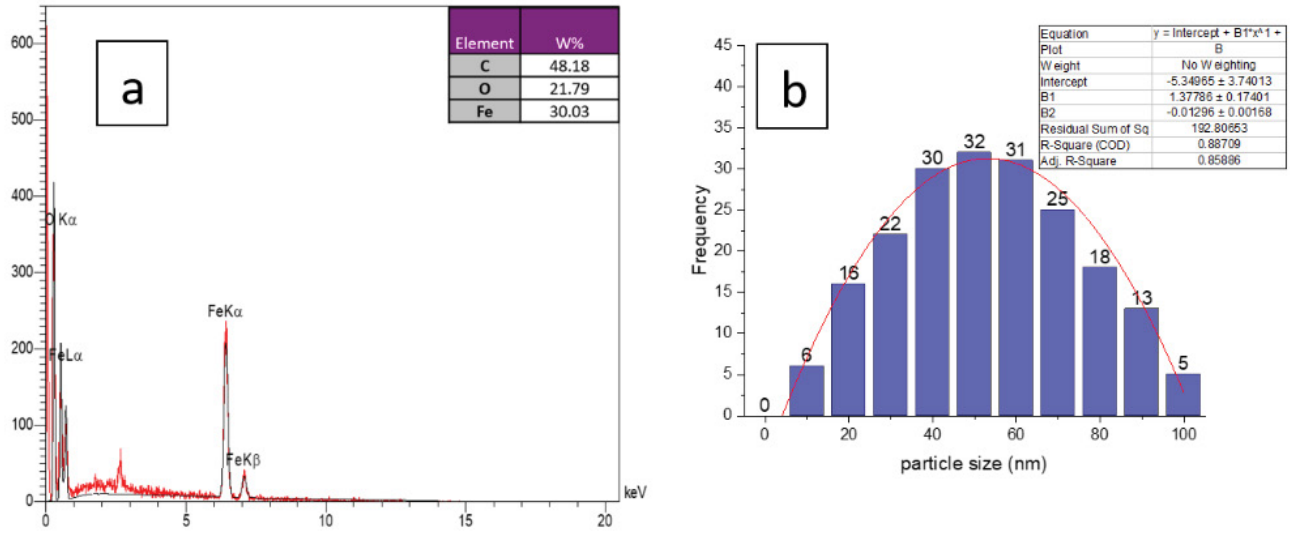

Fig. 5. (a) EDS data of MAC and (b) particle size distribution.

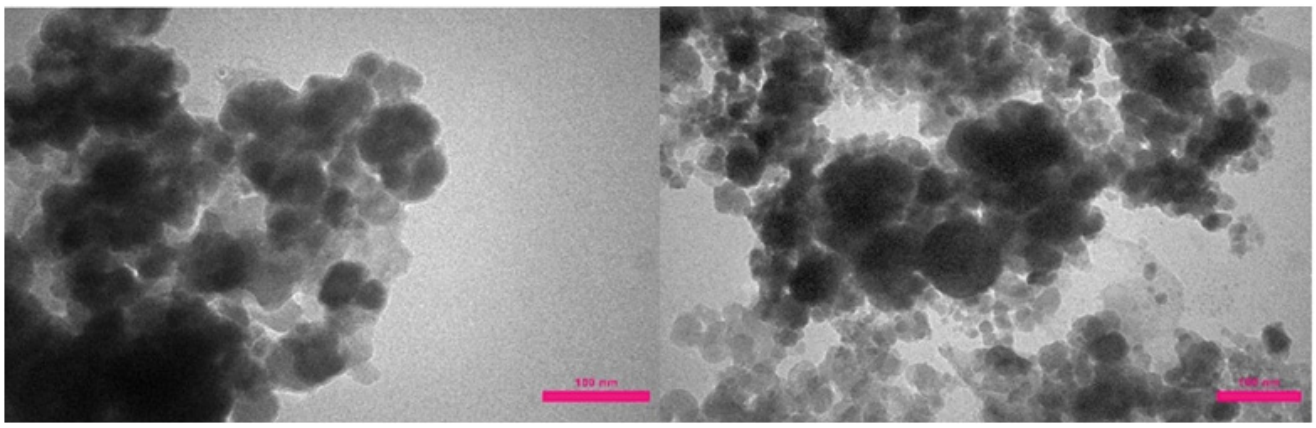

Fig. 6. TEM image of synthesized adsorbent.

Table 1
BET results

Sample	a_g (m^2 g^{-1})	V_m (cm^3(STP) g^{-1})	Total pore volume (cm^3 g^{-1})	Mean pore diameter (nm)
MAC	111.06	25.515	0.6971	25.108
Activated carbon	193.12	44.371	0.9703	20.096

the optimum pH was set to 8. Similar studies showed that at higher pH values (5–9) ATZ exists as a neutral molecule and therefore ATZ will have hydrophilic interaction with composite and the hydrogen bonds make the adsorption favorable [52].

3.2.2. Effect of contact time

The impact of reaction time (0–400 min) and ATZ removal at pH = 8 and 1 g L^{-1} of adsorbent dosage are shown in Fig. 11. The adsorption took place in a rapid step followed by a gradual stage for all concentrations owing to the driving force decrement caused by adsorbate reduction over time [53]. The equilibrium time (T_e) and concentration (C_e) for 5, 10, 15, 20, and 25 mg L^{-1} of ATZ are presented in Table 3. The T_e was achieved 220 and 240 min for 5–15 mg L^{-1} and 20, 25 mg L^{-1} respectively. Accumulation of ATZ molecules on the adsorbent surface and their steric hindrance and electrostatic repulsion will increase the equilibrium time. The optimal reaction time for ATZ adsorption process was considered 220 min.

3.2.3. Effect of adsorbent dosage

Calculating the optimum composite dosage accomplished by introducing 0.01, 0.02, 0.05, 0.1, 0.15 and 0.2 g

of adsorbent to series of conical flasks containing 100 mL of ATZ solution with 20 mg L^{-1} concentration. Flasks were placed on a shaker and reaction was done with speed of 250 rpm for 220 min. According to Fig. 12a monitoring concentration at 10 min intervals shows highest ATZ removal with 1.5 g L^{-1} of adsorbent dosage and resulted in complete removal. In as much as additive amounts of adsorbent to the solution, raise the numbers of active adsorption site [54]. On the contrary, considering the plot 12b, exceeding the adsorbent amounts to 2 g L^{-1}, reduces the composite activity and removal efficiency to 94% through overlapping and obstruction of pores [55]. The 1 g L^{-1} was selected as the ideal dosage and identical to the researches presented in [35,55]. The explanation for the lower adsorbent dosage (0.1 g L^{-1}) in the studies of [53,54], is the lower initial ATZ concentration in addition to using commercial AC as catalyst support which has higher surface area with type I/II BET isotherm that strongly supports multilayer adsorption. Fig. 13a illustrates a comparison between the adsorption capacity of Fe_3O_4 and synthesized magnetic activated carbon (MAC) which confirms the effect of AC on adsorption capacity. The adsorption capacity of MAC and AC is depicted in Fig. 13b which shows the higher power of the AC for adsorbing the pollutant.

3.2.4. Effect of initial ATZ concentration

The effect of different initial ATZ concentrations at a constant dosage of adsorbent on removal efficiency is illustrated in Fig. 14 and demonstrates a reduction in adsorption capability from 80% to 61% by increasing concentration from 5 to 25 mg L^{-1} respectively which is due to the filling up the adsorption sites. However, the adsorption capacity has increased. The best initial concentration was selected 15 mg L^{-1}.

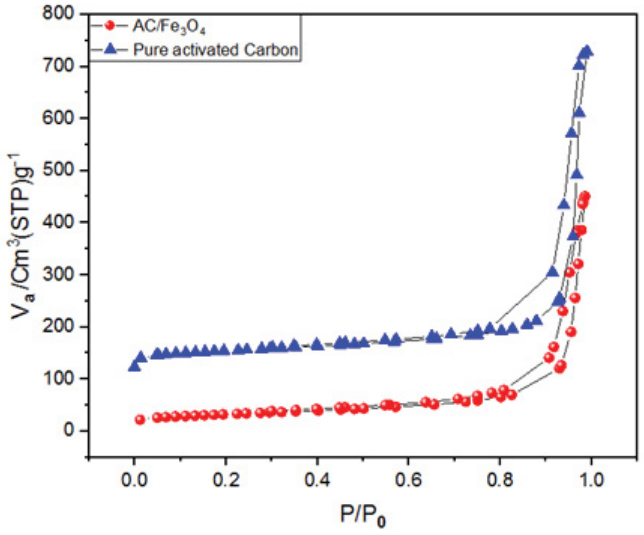

Fig. 7. Adsorption/desorption at 77.3°K for composite and scrap tire charcoal.

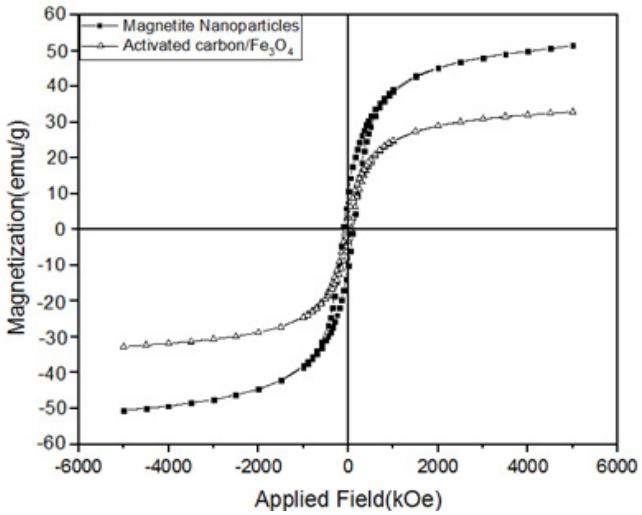

Fig. 8. Hysteresis loop of magnetite and magnetic adsorbent.

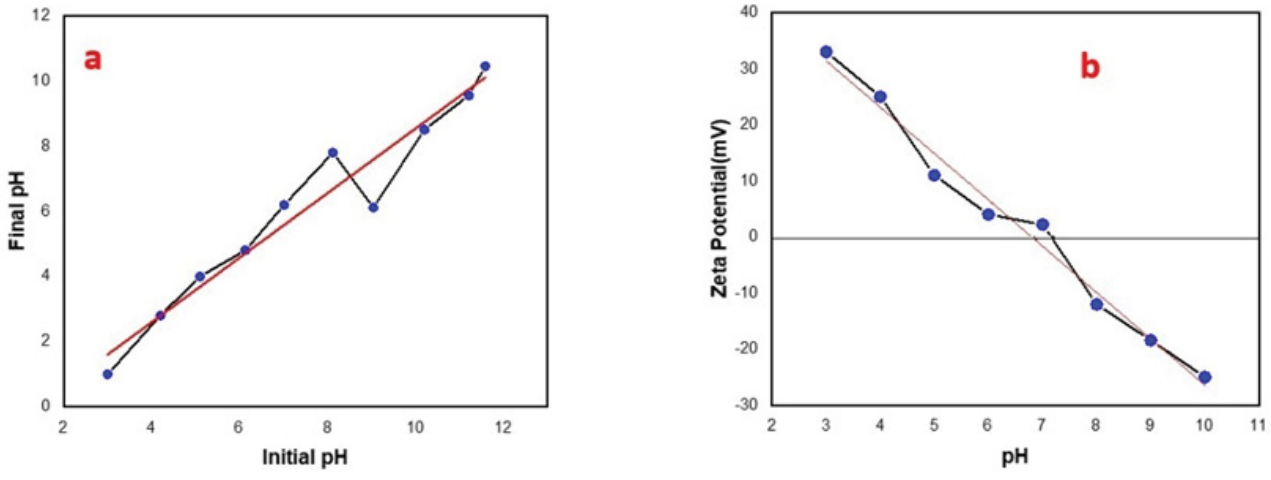

Fig. 9. (a) Plot of pH_{zpc} and (b) zeta potential variations at different pH values.

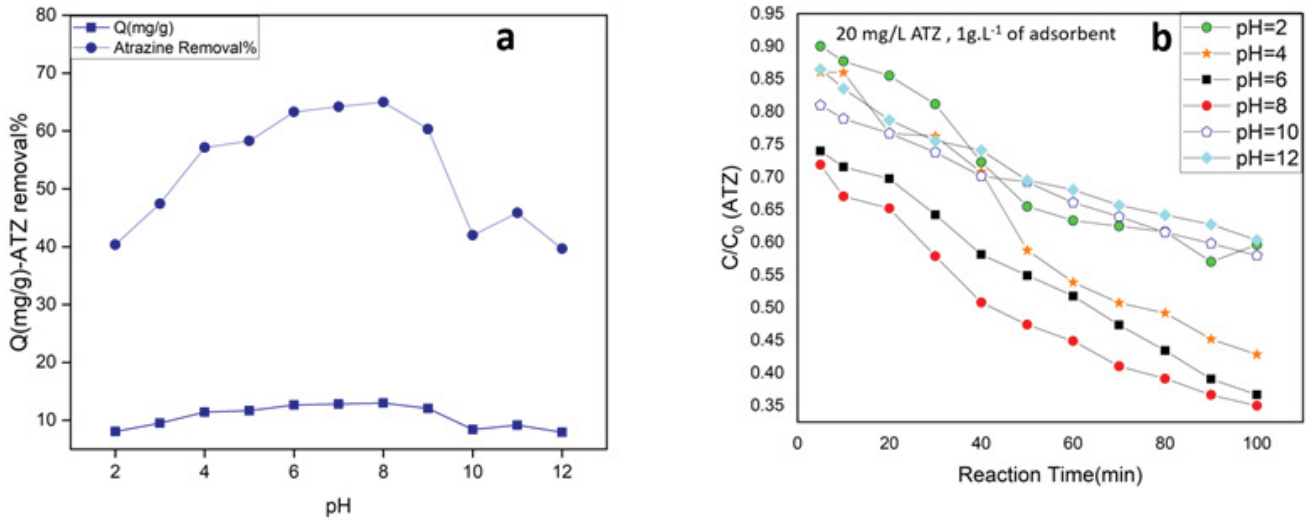

Fig. 10. (a) Variation of adsorption and removal percentage against pH and (b) fluctuations of concentration vs. time in various pH values.

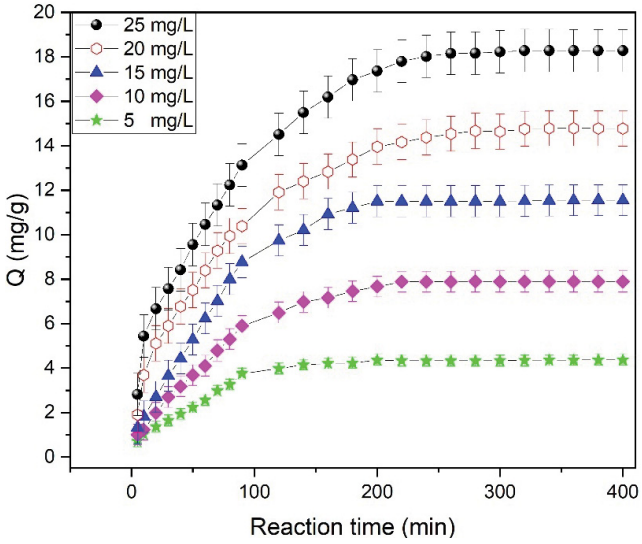

Fig. 11. Effect of contact time on adsorption of ATZ by MAC.

Table 2
Magnetic properties of magnetite and magnetic composite

Sample	Magnetization Ms (emu g^{-1})	Remanence Mr (emu g^{-1})	Coercivity Hc Qe
Fe_3O_4	55.68	0.21	0.41
Fe_3O_4/AC	36.43	1.2	2.44

3.3. Adsorption isotherms

The higher coefficient of Langmuir model (K_L) the higher correlation of adsorption/desorption. Moreover, the separation factor (R_L = 1/(1 + K_LC_0) states that the adsorption is unfavorable if $R_L > 1$, favorable if $0 < R_L < 1$, and irreversible with $R_L = 0$ [56]. The constant K_f is an approximate indicator of adsorption capacity, while $1/n$ is a function of the strength of adsorption in the adsorption process and represents the heterogeneity. The favorable sorption will happen if the intensity value (n) lies between 2 and 10, $1 < n < 2$ moderate adsorption and for $n < 1$ poor adsorption will take place [57]. Considering the results presented in Table 4 the Langmuir R_L coefficient for all concentration obtained between 0 and 1 which shows favorable adsorption while the n value for the Freundlich approached to 1.28 and indicates moderate adsorption. Fig. 15a and b shows that the Langmuir correlation coefficient (R^2) was 0.9995 and higher than that of Freundlich with R^2 = 0.996 which states that the sorption occurred on homogenous sites more than heterogenous ones, and consequently the type of adsorption was monolayer.

Table 3
Equilibrium time and concentration data

Concentration (ppm)	C_e (mg L^{-1})	Volume (L)	W(g) adsorbent	pH	T (°K)	Q_e (mg g^{-1})	Atrazine removal
5	0.99	0.1	0.1	8	293	4.01	80
10	2.1	0.1	0.1	8	293	7.9	79
15	3.5	0.1	0.1	8	293	11.5	76
20	5.21	0.1	0.1	8	293	14.79	74
25	6.72	0.1	0.1	8	293	18.28	73

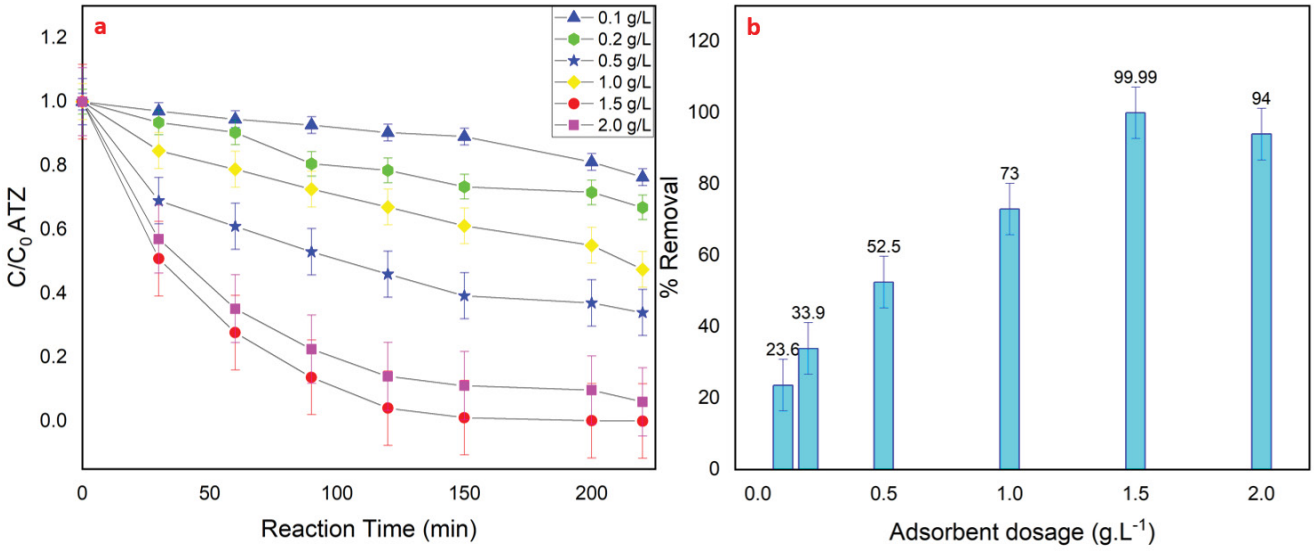

Fig. 12. (a and b) impact of adsorbent dosage on ATZ removal [C_0 = 20 mg L^{-1}, pH = 8, T = 220 min].

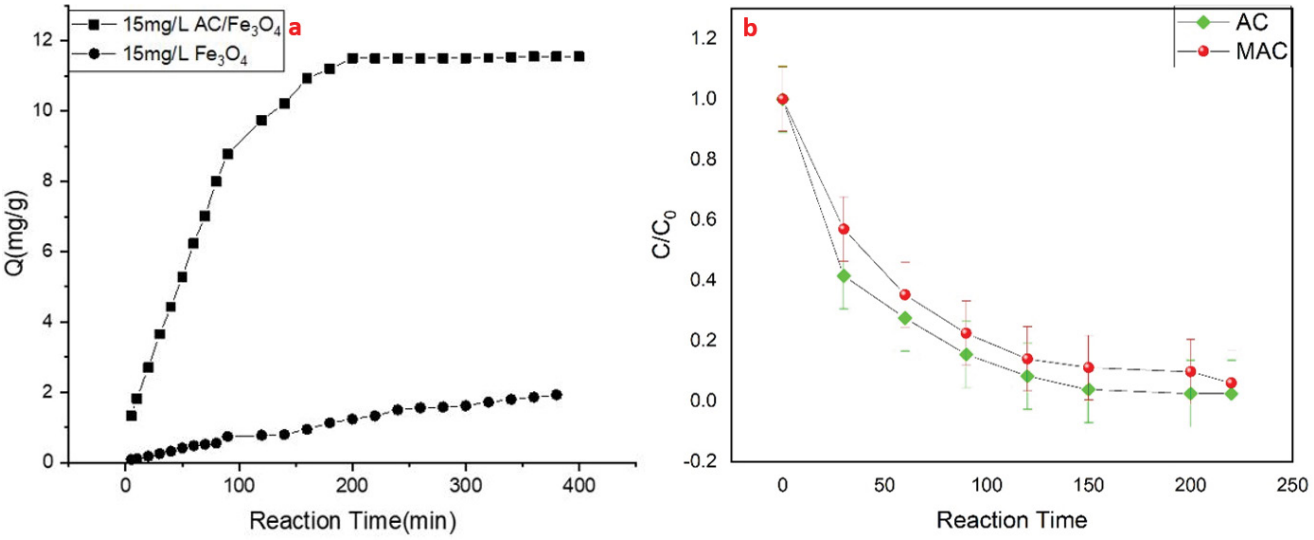

Fig. 13. Adsorption capacity of (a) MAC and magnetite particles and (b) MAC and AC.

However, the adsorption for ATZ cannot be clarified by the Langmuir model while the ATZ is a big molecule. On the other hand, the adsorption behavior of Fe_3O_4 nanoparticles presented in Fig. 13a was negligible compared to the composite and therefore the adsorption could be attributed to the π-π bonds and electrostatic interaction between the adsorbent and adsorbate [37]. The maximum adsorption capacity of the ATZ on MAC is 44.62 mg g^{-1}. A comparison between diverse adsorbents for adsorption of ATZ is provided in Table 5 and demonstrates a good performance for MAC.

3.4. Adsorption kinetics

Pseudo-first-order and pseudo-second-order kinetic model's data are given in Table 6 and considering the correlation factors the pseudo-second-order model is better fitting for adsorption process, hence the reaction is of physicochemical type. Additionally, the calculated adsorption capacities (q_{cal}) deviations from experimental amounts (q_{exp}) are lesser in the pseudo-second-order rather than pseudo-first-order, and consequently it could be inferred that the chemisorption is the rate limiting factor [62].

3.5. Adsorbent regeneration

The recyclability of adsorbent was done by using 20 mL of methanol as the desorption reagent. Due to the leaching of Fe ions in acidic media, 0.1 M NaOH solution was used to fix the pH of wash water at 12. Fig. 16 shows the reduction of composite activity after 3 cycles of adsorption and desorption. Reducing the activity from 93% to 81%

shows the presence of Fe_2O_3 on the adsorbent surface and releasing Fe ions to the solution. Fig. 4c shows the SEM of regenerated adsorbent and it can be observed that the iron oxide density has increased on the surface and the active sites numbers were decreased which can lead to reduce the efficiency [54].

4. Conclusion

The magnetic composite AC/Fe_3O_4 have been synthesized by wet chemical synthesis and its application for atrazine removal was studied. Characterization of composite showed mesoporous structure and the presence of magnetite (Fe_3O_4) with proper size distribution in the carbon lattice was confirmed. The small quantities of coercivity and remanence magnetization in the composite indicated super-paramagnetic property. Performed experiments for ATZ removal exhibited a good proficiency for

Table 4
Langmuir and Freundlich correlation data

Langmuir isotherm			
q_m (mg g^{-1})	K_L (L mg^{-1})	R^2	R_L
44.61816	0.100073	0.9995	0.285564–0.666503
Freundlich			
K_f (mg/g (L mg)$^{1/n}$)	$1/n$	R^2	
4.200220902	0.780113	0.9956	

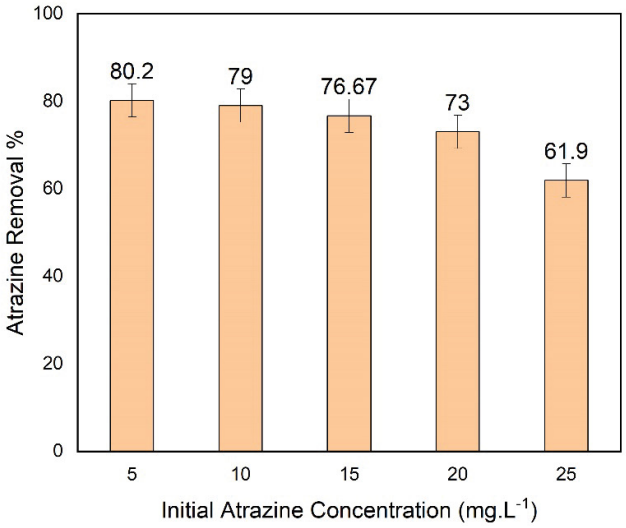

Fig. 14. ATZ removal in different initial concentrations [pH = 8, 1 g L^{-1} of adsorbent].

Table 5
Comparison of maximum capacity of ATZ on various adsorbents

Adsorbent	Pollutants	Temperature	Dose (g L^{-1})	pH	Q_{exp} max. (mg g^{-1})	References
AC/MgO/ZnO	ATZ	20	2	5	29.8% ± 0.7%	[26]
Nanoporous carbon	ATZ	25			51	[27]
Fe_3O_4/graphene nanocomposite	ATZ	20	0.5	5	54.8	[30]
Magnetic Fe_3O_4@SiO_2	ATZ	20	1		0.053	[52]
Zeolitic imidazolate framework-8(ZIF8), UIO 67	ATZ	25	2.4	6.9	6.78, 10.96	[58]
Unmodified bentonite clay (UBC)	ATZ	30	0.1	12	76.92	[59]
Acid modified bentonite clay (ABC)				12	125	
Base modified bentonite clay (BBC)				7	111.11	
Chitosan-modified sepiolite	ATZ	65	2	6.5	17.92	[60]
Wood industry biochar	ATZ	20	2	5.8	3.333	[61]
MAC	ATZ	20	1	8	44.62	This study

Table 6
Pseudo-first-order and pseudo-second-order reactions data

Initial atrazine concentration (mg L^{-1})	Pseudo-first-order				Pseudo-second-order		
	$Q_{e,exp}$ (mg g^{-1})	$Q_{e,cal}$ (mg g^{-1})	k_1 (1/min)	R^2	$Q_{e,cal}$ (mg g^{-1})	k_2 (g/(mg min))	R^2
5	4.01	1.33	0.01666	0.8264	4.32	0.0099	000.996
10	7.9	12.89	0.02179	0.9786	9.54	0.0016	0.9929
15	11.5	17.068	0.0196	0.9772	13.91	0.00107	0.9924
20	14.79	31.89	0.01849	0.9741	19.3862	0.000462	0.9949
25	18.28	45.46	0.00413	0.999	28.37	0.000188	0.9902

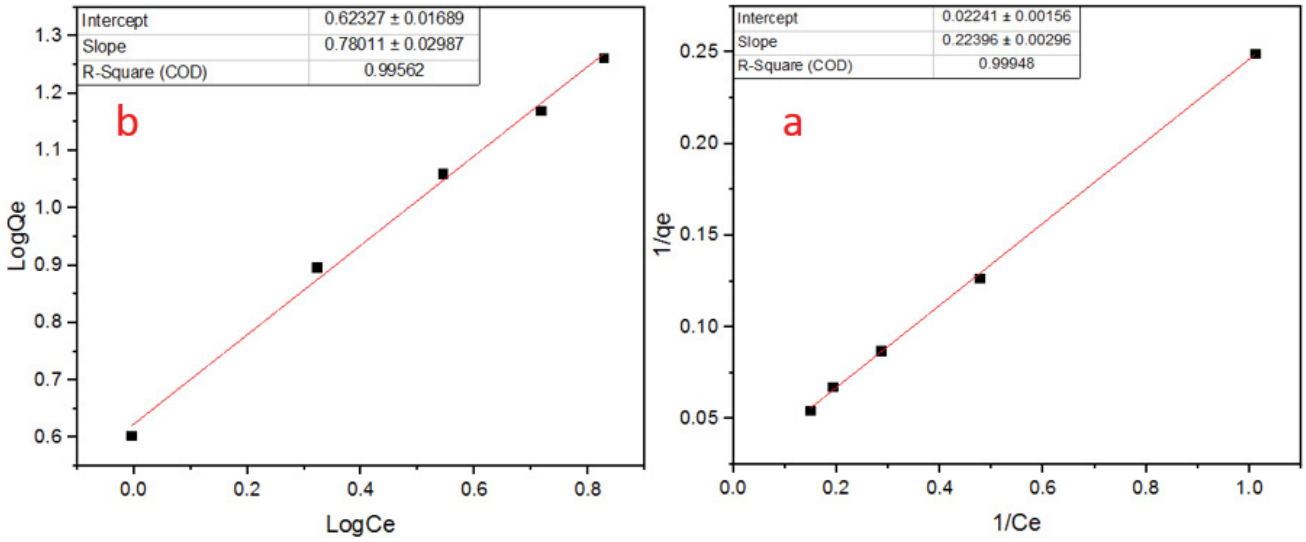

Fig. 15. (a) Langmuir and (b) Freundlich models for ATZ adsorption on AC/Fe_3O_4 adsorbent.

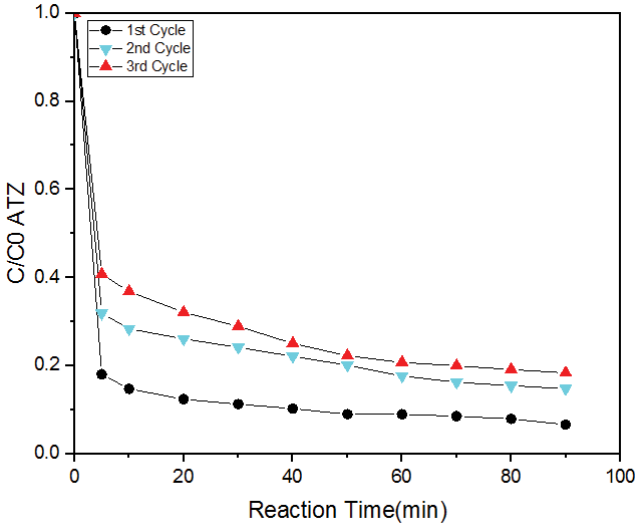

Fig. 16. The changes in adsorbent activity after 3 cycles [ATZ] = 15 ppm, adsorbent dosage = 1 g L^{-1}.

ATZ adsorption. In comparison to the identical studies, this research showed that scrap tire charcoal with lower surface area, had acceptable performance and it was quite capable of removing organic pollutions. The adsorbent activity after three cycle had a minute reduction that indicates the ability of the composite to be regenerated and reused. In conclusion, ATZ adsorption with activate carbon derived from waste tire is a promising method and we investigated the s-triazines oxidation through heterogeneous reaction by this adsorbent in another study.

Acknowledgement

The authors would like to express their thanks to the laboratory staff and faculty of the Department of Health Environmental Engineering of Mazandaran University of Medical Science. We also thanks Mazandaran Health Center laboratory for their collaboration.

Funding

This research did not receive any specific grant from funding agencies in the public, commercial, or not-for-profit sectors

References

[1] R. Eisler, Eisler's Encyclopedia of Environmentally Hazardous Priority Chemicals, Elsevier Science, Amsterdam, The Netherlands, 2007. Available at: https://books.google.com/books?id=B3qXQswP8zIC
[2] L. Jowa, R. Howd, Should atrazine and related chlorotriazines be considered carcinogenic for human health risk assessment?, J. Environ. Sci. Health., Part C Environ. Carcinog. Ecotoxicol. Rev., 29 (2011) 91–144.
[3] M. Graymore, F. Stagnitti, G. Allinson, Impacts of atrazine in aquatic ecosystems, Environ. Int., 26 (2001) 483–495.
[4] J.J. Zhang, Y.C. Lu, J.J Zhang, L.R. Tan, H. Yang, Accumulation and toxicological response of atrazine in rice crops, Ecotoxicol. Environ. Saf., 102 (2014) 105–112.
[5] M. Zhu, L. Wang, Y. Wang, J. Zhou, J. Ding, W. Li, Y. Xin, S. Fan, Z. Wang, Y. Wang, Biointeractions of herbicide atrazine with human serum albumin: UV-Vis, fluorescence and circular dichroism approaches, Int. J. Environ. Res. Public Health, 15 (2018) 116, doi: 10.3390/ijerph15010116.
[6] M.A. Baghapour, S. Nasseri, Z. Derakhshan, Atrazine removal from aqueous solutions using submerged biological aerated filter, J. Environ. Health Sci. Eng., 11 (2013) 1–9, doi: 10.1186/2052-336X-11-6.
[7] P. Boffetta, H.O. Adami, C. Berry, J.S. Mandel, Atrazine and cancer: a review of the epidemiologic evidence, Eur. J. Cancer Prev., 22 (2013) 169–180.
[8] D.W. Gammon, C.N. Aldous, W.C. Carr, J.R. Sanborn, K.F. Pfeifer, A risk assessment of atrazine use in California: human health and ecological aspects, Pest. Manage. Sci., 61 (2005) 331–355.
[9] Z. Derakhshan, M.H. Ehrampoush, A.H. Mahvi, M. Dehghani, M. Faramarzian, H. Eslami, A comparative study of hybrid membrane photobioreactor and membrane photobioreactor for simultaneous biological removal of atrazine and CNP from wastewater: a performance analysis and modeling, Chem. Eng. J., 355 (2019) 428–438.

[10] X. Wu, H. He, W.L. Yang, J. Yu, C. Yang, Efficient removal of atrazine from aqueous solutions using magnetic *Saccharomyces cerevisiae* bionanomaterial, Appl. Microbiol. Biotechnol., 102 (2018) 7597–7610.
[11] J. Yu, H. He, W.L. Yang, C. Yang, G. Zeng, X. Wu, Magnetic bionanoparticles of *Penicillium* sp. Yz11-22N2 doped with Fe_3O_4 and encapsulated within PVA-SA gel beads for atrazine removal, Bioresour. Technol., 260 (2018) 196–203.
[12] P.K. Ghosh, L. Philip, M. Bandyopadhyay, Anaerobic treatment of atrazine bearing wastewater, J. Environ. Sci. Health., Part B, 36 (2001) 301–316.
[13] S. Marcacci, A Phytoremediation Approach to Remove Pesticides (Atrazine and Lindane) From Contaminated Environment, Thesis, EPFL (École polytechnique fédérale de Lausanne), Lausanne, 2004, doi: 10.5075/epfl-thesis-2950.
[14] P. Luis, M. Saquib, C. Vinckier, B. Van der Bruggen, Effect of membrane filtration on ozonation efficiency for removal of atrazine from surface water, Ind. Eng. Chem. Res., 50 (2011) 8686–8692.
[15] N.B. Turan, H.S. Erkan, A. Çaglak, S. Bakırdere, G.O. Engin, Optimization of atrazine removal from synthetic groundwater by electrooxidation process using titanium dioxide and graphite electrodes, Sep. Sci. Technol., 55 (2020) 3036–3045.
[16] A. Bo´dalo, G. Leo´n, A.M. Hidalgo, M. Go´mez, M.D. Murcia, P. Blanco, Atrazine removal from aqueous solutions by nanofiltration, Desal. Water Treat., 13 (2010) 143–148.
[17] C. Petrier, B. David, S. Laguian, Ultrasonic degradation at 20 kHz and 500 kHz of atrazine and pentachlorophenol in aqueous solution: preliminary results, Chemosphere, 32 (1996) 1709–1718.
[18] M.S. Karmacharya, V.K. Gupta, I. Tyagi, S. Agarwal, V.K. Jha, Removal of As(III) and As(V) using rubber tire derived activated carbon modified with alumina composite, J. Mol. Liq., 216 (2016) 836–844.
[19] W. Ahmad, S. Qaiser, R. Ullah, B. Mohamed Jan, M.A. Karakassides, C.E. Salmas, G. Kenanakis, R. Ikram, Utilization of tires waste-derived magnetic-activated carbon for the removal of hexavalent chromium from wastewater, Materials (Basel, Switzerland), 14 (2020) 34, doi: 10.3390/ma14010034.
[20] H. Tabarinia, M. Zazouli, Z. Yousefi, L.R. Kalankesh, J. Charati, Response surface methodology, modeling to improve mercury removal from aqueous solutions using L-cysteine functionalized multi-walled carbon nanotubes, Global Nest J., 21(2019) 64–69.
[21] M. Zazouli, D. Balarak, F. Kariminejad, F. Khosravi, Removal of fluoride from aqueous solution by using of adsorption onto modified *Lemna minor*: adsorption isotherm and kinetics study, J. Mazandaran Univ. Med. Sci., 24 (2014) 195–204.
[22] M. Zazouli, A. Azari, A. Dehghan, S. Salmani, R. Malekkolae, Adsorption of methylene blue from aqueous solution onto activated carbons developed from eucalyptus bark and *Crataegus oxyacantha* core, Water Sci. Technol., 74 (9) (2016) 2021–2035, https://doi.org/10.2166/wst.2016.287.
[23] E. Bazrafshan, A. Zarei, H. Nadi, M. Zazouli, Adsorptive removal of Methyl Orange and Reactive Red 198 dyes by *Moringa peregrina* ash, Indian J. Chem. Technol., 21 (2014) 105–113.
[24] M.A. Ebrahimzadeh, S. Mortazavi-Derazkola, M.A. Zazouli, Eco-friendly green synthesis and characterization of novel $Fe_3O_4/SiO_2/Cu_2O$–Ag nanocomposites using *Crataegus pentagyna* fruit extract for photocatalytic degradation of organic contaminants, J. Mater. Sci.: Mater. Electron., 30 (2019), doi: 10.1007/s10854-019-01440-8.
[25] B. Kakavandi, J. Salimi, A. Babaei, A. Takdastan, N. Alavi, A. Neisi, B. Ayoubi-Feiz, Modeling and optimization of nonylphenol removal from contaminated water media using a magnetic recoverable composite by artificial neural networks, Water Sci. Technol., 75 (2017) 1761–1775.
[26] M. Shirmardi, N. Alavi, E.C. Lima, A. Takdastan, A.H. Mahvi, A.A. Babaei, Removal of atrazine as an organic micro-pollutant from aqueous solutions: a comparative study, Process Saf. Environ. Prot., 103 (2016) 23–35.
[27] C.P. Amézquita-Marroquín, P. Torres-Lozada, L. Giraldo, P.D. Húmpola, E. Rivero, P.S. Poon, J.C. Moreno-Piraján, Sustainable production of nanoporous carbons: kinetics and equilibrium studies in the removal of atrazine, J. Colloid Interface Sci., 562 (2020) 252–267.
[28] F. Cecen, Ö. Aktas, Activated Carbon for Water and Wastewater Treatment: Integration of Adsorption and Biological Treatment, 2011. Available at: https://books.google.com/books?id=ubVxmXZ0j8wC
[29] S.B. Butt, M. Innayat, M. Riaz, A. Mahmood, Activated Carbon From Scrap Tires for Water Purification, Int. Wedc Conference, Water, Engineering and Development Centre, 24 (1998) 340–342.
[30] P.K. Boruah, B. Sharma, N. Hussain, M.R. Das, Magnetically recoverable Fe_3O_4/graphene nanocomposite towards efficient removal of triazine pesticides from aqueous solution: investigation of the adsorption phenomenon and specific ion effect, Chemosphere, 168 (2017) 1058–1067.
[31] G. Liu, T. Li, X. Yang, Y. She, M. Wang, J. Wang, M. Jin, Competitive fluorescence assay for specific recognition of atrazine by magnetic molecularly imprinted polymer based on Fe_3O_4-chitosan, Carbohydr. Polym., 137 (2016) 75–81.
[32] G. Liu, X. Yang, T. Li, Y. She, S. Wang, J. Wang, H. Shao, Preparation of a magnetic molecularly imprinted polymer using g-C_3N_4-Fe_3O_4 for atrazine adsorption, Mater. Lett., 160 (2015) 472–475.
[33] V.K. Gupta, B. Gupta, A. Rastogi, S. Agarwal, A. Nayak, A comparative investigation on adsorption performances of mesoporous activated carbon prepared from waste rubber tire and activated carbon for a hazardous azo dye—Acid Blue 113, J. Hazard. Mater., 186 (2011) 891–901.
[34] J. Rios-Hurtado, E. Muzquiz-Ramos, A. Zugasti-Cruz, D. Hernández, Mechanosynthesis as a simple method to obtain a magnetic composite (activated carbon/Fe_3O_4) for hyperthermia treatment, J. Biomater. Nanobiotechnol., 7 (2016) 19–28.
[35] C.S. Castro, M.C. Guerreiro, M. Gonçalves, L.C.A. Oliveira, A.S. Anastácio, Activated carbon/iron oxide composites for the removal of atrazine from aqueous medium, J. Hazard. Mater., 164 (2009) 609–614.
[36] G. Tan, Y. Mao, H. Wang, M. Junaid, N. Xu, Comparison of biochar- and activated carbon-supported zerovalent iron for the removal of Se(IV) and Se(VI): influence of pH, ionic strength, and natural organic matter, Environ. Sci. Pollut. Res., 26 (2019) 21609–21618.
[37] S. Li, Y. Gong, Y. Yang, C. He, L. Hu, L. Zhu, D. Shu, Recyclable CNTs/Fe_3O_4 magnetic nanocomposites as adsorbents to remove bisphenol A from water and their regeneration, Chem. Eng. J., 260 (2015) 231–239.
[38] Z. Bai, Q. Yang, J. Wang, Catalytic ozonation of dimethyl phthalate using Fe_3O_4/multi-wall carbon nanotubes, Environ. Technol., 38 (2017) 2048–2057.
[39] K. Manna, S.K. Srivastava, Fe_3O_4@carbon@polyaniline trilaminar core–shell composites as superior microwave absorber in shielding of electromagnetic pollution, ACS Sustainable Chem. Eng., 5 (2017) 10710–10721.
[40] J. Tang, J. Wang, Fe_3O_4-MWCNT magnetic nanocomposites as efficient fenton-like catalysts for degradation of sulfamethazine in aqueous solution, ChemistrySelect, 2 (2017) 10727–10735.
[41] Z. Chen, J. Wang, Z. Pu, Y. Zhao, D. Jia, H. Chen, T. Hayat, Synthesis of magnetic Fe_3O_4/CFA composites for the efficient removal of U(VI) from wastewater, Chem. Eng. J., 320 (2017) 448–457.
[42] Z.T. Li, B. Lin, L.W. Jiang, E.C. Lin, J. Chen, S.J. Zhang, D.H. Li, Effective preparation of magnetic superhydrophobic Fe_3O_4/PU sponge for oil–water separation, Appl. Surf. Sci., 427 (2018) 56–64.
[43] S. Asgari, Z. Fakhari, S. Berijani, Synthesis and characterization of Fe_3O_4 magnetic nanoparticles coated with carboxymethyl chitosan grafted sodium methacrylate, J. Nanostruct., 4 (2014) 55–63.
[44] S.C. Rodrigues, M.C. Silva, J.A. Torres, M.L. Bianchi, Use of magnetic activated carbon in a solid phase extraction procedure for analysis of 2,4-dichlorophenol in water samples, Water Air Soil Pollut., 231 (2020) 1–13.
[45] K.S.W. Sing, D.H. Everett, R.A.W. Haul, L. Moscou, R.A. Pierotti, J. Rouquerol, T. Siemieniewska, Reporting physisorption data

for gas/solid systems with special reference to the determination of surface area and porosity, Pure Appl. Chem., 57 (1985) 603–619.
[46] M.H. Do, N.H. Phan, T.D. Nguyen, T.T.S. Pham, T.T.T. Vu, T.K.P. Nguyen, Activated carbon/Fe_3O_4 nanoparticle composite: fabrication, methyl orange removal and regeneration by hydrogen peroxide, Chemosphere, 85 (2011) 1269–1276.
[47] N. Yang, S. Zhu, D. Zhang, S. Xu, Synthesis and properties of magnetic Fe_3O_4-activated carbon nanocomposite particles for dye removal, Mater. Lett., 62 (2008) 645–647.
[48] P. Strachowski, W. Kaszuwara, M. Bystrzejewski, A novel magnetic composite adsorbent of phenolic compounds based on waste poly(ethylene terephthalate) and carbon-encapsulated magnetic nanoparticles, New J. Chem., 41 (2017) 12617–12630.
[49] D.W. Wang, F. Li, G.Q. Lu, H.M. Cheng, Synthesis and dye separation performance of ferromagnetic hierarchical porous carbon, Carbon, 46 (2008) 1593–1599.
[50] C. Anyika, N.A.M. Asri, Z.A. Majid, A. Yahya, J. Jaafar, Synthesis and characterization of magnetic activated carbon developed from palm kernel shells, Nanotechnol. Environ. Eng., 2 (2017) 16, doi: 10.1007/s41204-017-0027-6.
[51] N.Y. Rachel, B. Abdelaziz, K. Daouda, N.N. Julius, D.D.E. Gaelle, Y. Abdelrani, K.M. Joseph, Optimization study of the removal of atrazine from aqueous solution on to composite activated carbon-silver using response surface methodology, Mater. Sci. Appl., 8 (2017) 258–272.
[52] H.F. Men, H.Q. Liu, Z.L. Zhang, J. Huang, J. Zhang, Y.Y. Zhai, L. Li, Synthesis, properties and application research of atrazine Fe_3O_4@SiO_2 magnetic molecularly imprinted polymer, Environ. Sci. Pollut. Res., 19 (2012) 2271–2280.
[53] A.A. Morales-Pérez, C. Arias, R.M. Ramírez-Zamora, Removal of atrazine from water using an iron photo catalyst supported on activated carbon, Adsorption, 22 (2016) 49–58.
[54] L. Yu, X. Yang, Y. Ye, D. Wang, Efficient removal of atrazine in water with a Fe_3O_4/MWCNTs nanocomposite as a heterogeneous Fenton-like catalyst, RSC Adv., 5 (2015) 46059–46066.
[55] T.B. Benzaquén, N.I. Cuello, O.M. Alfano, G.A. Eimer, Degradation of atrazine over a heterogeneous photo-fenton process with iron modified MCM-41 materials, Catal. Today, 296 (2017) 51–58.
[56] V. Makrigianni, A. Giannakas, Y. Deligiannakis, I. Konstantinou, Adsorption of phenol and methylene blue from aqueous solutions by pyrolytic tire char: equilibrium and kinetic studies, J. Environ. Chem. Eng., 3 (2015) 574–582.
[57] B. Kakavandi, A. Jonidi, R. Rezaei, S. Nasseri, A. Ameri, A. Esrafily, Synthesis and properties of Fe_3O_4-activated carbon magnetic nanoparticles for removal of aniline from aqueous solution: equilibrium, kinetic and thermodynamic studies, Iran. J. Environ. Health Sci. Eng., 10 (2013) 1–9.
[58] I. Akpinar, A.O. Yazaydin, Adsorption of atrazine from water in metal–organic framework materials, J. Chem. Eng. Data, 63 (2018) 2368–2375.
[59] O.J. Ajala, F.O. Nwosu, R.K. Ahmed, Adsorption of atrazine from aqueous solution using unmodified and modified bentonite clays, Appl. Water Sci., 8 (2018) 1–11, doi: 10.1007/s13201-018-0855-y.
[60] H. Liu, W. Chen, B. Cui, C. Liu, Enhanced atrazine adsorption from aqueous solution using chitosan-modified sepiolite, J. Cent. South Univ., 22 (2015) 4168–4176.
[61] M. Fruehwirth, M. Sbizzaro, D.M. Rosa, S.C. Sampaio, R.R.D. Reis, Adsorption of atrazine by biochars produced from byproducts of the wood industry, Eng. Agric., 40 (2020) 769–776.
[62] Y.S. Ho, G. McKay, A comparison of chemisorption kinetic models applied to pollutant removal on various sorbents, Process Saf. Environ. Prot., 76 (1998) 332–340.